Journal of Nuclear Materials 463 (2015) 276–279

Contents lists available at ScienceDirect

Journal of Nuclear Materials

journal homepage: www.elsevier.com/locate/jnucmat

OEDGE modeling of outer wall erosion in NSTX and the effect of changes in neutral pressure

J.H. Nichols *[,1], M.A. Jaworski, R. Kaita, T. Abrams, C.H. Skinner, D.P. Stotler

Princeton Plasma Physics Laboratory, Princeton, NJ 08543, USA

ARTICLE INFO

Article history:
Available online 7 November 2014

ABSTRACT

Gross erosion from the outer wall is expected to be a major source of impurities for high power fusion devices due to the low redeposition fraction. Scaling studies of sputtering from the all-carbon outer wall of NSTX are reported. It is found that wall erosion decreases with divertor plasma pressure in low/mid temperature regimes, due to increasing divertor neutral opacity. Wall erosion is found to consistently decrease with reduced recycling coefficient, with outer target recycling providing the largest contribution. Upper and lower bounds are calculated for the increase in wall erosion due to a low-field-side gas puff.

1. Introduction

Erosion of plasma-facing components (PFCs) provides an impurity source that can limit tokamak performance and material lifetimes. Erosion typically increases with increasing particle flux and energy, and thus these issues are expected to be exacerbated as fusion devices scale up in size, power, and duty factor [1].

Prompt redeposition (the ionization and deposition of a sputtered neutral within one impurity gyroradius) leads to lower net erosion compared to gross erosion, but this process typically requires high plasma density and thus is only significant near the strike points of a diverted tokamak [2]. Migration of sputtered impurities from other locations in the machine can also reduce net erosion, but experiments on JET [3,4], DIII-D [5], and ASDEX Upgrade [6] have shown that the dominant migration pathway is from the outer wall to the inner divertor target. Thus, the outer wall of a fusion device will likely be in a regime where the net erosion rate of the PFC surface is close to the gross erosion rate.

The present study aims to model the scaling of the gross erosion rate from the carbon outer wall of the National Spherical Torus Experiment (NSTX), using data from the 2010 NSTX campaign. In 2010 NSTX was operated with ATJ graphite walls and the Liquid Lithium Divertor (LLD) outer target, a porous molybdenum surface that could be filled with lithium evaporated via the LITER system [7]. NSTX-Upgrade [8] will initially operate with graphite PFCs on both the walls and targets, so simulations with all-carbon PFCs are still of interest for investigating erosion in the spherical torus configuration. Carbon also has mechanical properties that may make it an attractive PFC choice for next-step devices [9].

The flux of ions striking the outer wall in NSTX is expected to be negligible due to the large gap between the plasma and PFC contour ($R_{gap,mid}/\lambda_{SOL} \sim 5$). The assumption of negligible ion flux to the walls will be further tested in NSTX-U via extended coverage of tile-mounted Langmuir probes. In the absence of ions, erosion profiles along the wall are determined by the flux and energy of neutrals striking the PFCs. D^0 neutrals recycled from the PFCs obtain wall-directed momentum via resonant charge exchange (CX) collisions with energetic D^+ ions, and this CX rate is proportional to the local neutral density. The kinetic Monte Carlo neutral code EIRENE [10] simulates hydrogenic neutral transport, including the ionization, recombination, and CX processes that are key to calculating neutral fluxes out of the plasma. EIRENE has been coupled to the 2D fluid background solver OSM (Onion Skin Model) and the impurity Monte Carlo transport code DIVIMP as part of the OEDGE suite [11], which is utilized in the present study.

2. Simulation setup

The plasma background input to EIRENE is reconstructed using data from NSTX discharge 139396 at 600 ms, a lower single null, low-triangularity, H-mode plasma with $B_t = 0.45$ T, $I_p = 0.8$ MA, $P_{NBI} = 4$ MW, $\langle n_e \rangle = 6.5 \times 10^{21}$ m^{-3}, and $B \times \nabla B$ drift toward the x-point. The outer strike point is located on the outer target, and radial profiles of target electron temperature and ion saturation current are obtained from the embedded High Density Langmuir Probe (HDLP) array [12]. A more complete discussion of this discharge can be found in [13].

* Corresponding author at: Princeton Plasma Physics Lab, MS30 C-Site, P.O. Box 451, Princeton, NJ 08543, USA.
E-mail address: jnichols@pppl.gov (J.H. Nichols).
[1] Presenting author.

http://dx.doi.org/10.1016/j.jnucmat.2014.10.094
0022-3115/

OSM solves for n_e, T_e, T_i, and the background flow velocity by solving four 1D fluid conservation equations (particle, electron energy, ion energy, and momentum) simultaneously along flux surface-aligned rings, using the Langmuir probe data as a boundary condition. OSM is iteratively coupled to EIRENE to include volumetric particle, energy, and momentum source terms in the calculation. Thomson scattering and charge exchange recombination spectroscopy data set plasma parameters inside the last closed flux surface.

Global neutral density and energy profiles are extracted from the final iteration of EIRENE. The D^0 pressure profile for the data-based plasma reconstruction, which serves as a baseline for the scaling studies, is shown in Fig. 1. As a validity check, Fig. 2 shows a radial slice through the outer midplane of the OEDGE-calculated D^0 and D_2 density compared to a local DEGAS 2 simulation of the same region, which is calibrated with the Edge Neutral Density Diagnostic (ENDD) [14]. The radial locations of steep gradient regions show good agreement between the two codes, and the magnitude of neutral densities in the far SOL agree within a factor of 2, which is close compared to the 10^5 range in neutral densities calculated by EIRENE.

Physical sputtering rates are calculated according to the energy- and angle-dependent formulae for deuterium on carbon from Eckstein [15]. Chemical sputtering is calculated according to the energy-dependent empirical formula of Garcia–Rosales and Roth, modified to reduce the yield at high incident fluxes and assuming a wall temperature of 300 K [16].

The inner divertor plasma of NSTX is poorly diagnosed, so no attempt is made in this work to comprehensively model the inner divertor leg. However, it is found that prescribing a wide range of inner divertor regimes, both attached and detached, has negligible effect on the erosion profile on the outer wall.

The following sections present scaling studies, where one aspect of the simulation is changed from the baseline case, and the plasma background is recomputed via OSM and EIRENE iteration. Of special interest is the outer wall-integrated mass loss rate, defined here as the chemically and physically sputtered carbon flux, fully toroidally integrated and integrated poloidally from the gap between the upper inner and outer divertors to the $\Psi_N = 1.03$ location of the lower outer divertor.

3. Dependence on divertor plasma pressure

This analysis investigates the scaling of gross erosion with power in the NSTX geometry, using divertor plasma pressure as a proxy for parallel power through the divertor sheath (power $\sim nT^{3/2}$) [17]. Plasma backgrounds are reconstructed via OSM/EIRENE from synthetic Langmuir probe data, generated by scaling the measured target profiles ($T_e = 4$–5 eV, $n_e = 0.5$–4×10^{20} m^{-3} peaked at the strike point) by a constant multiplier. Simulations are carried out

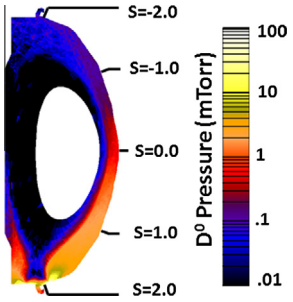

Fig. 1. Poloidal plot of the D^0 pressure, in mTorr, calculated by OEDGE for shot 139396@600 ms. Also shown is definition of wall-aligned poloidal coordinates.

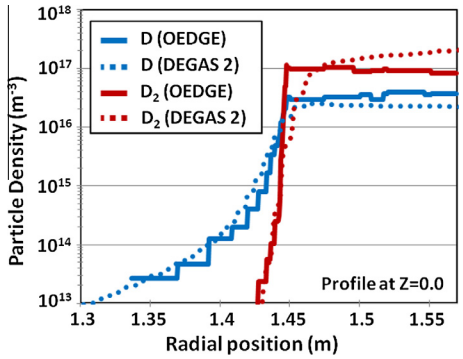

Fig. 2. Comparison of radial D (blue) and D_2 (red) density profiles at outer midplane for shot 139396@600 ms, as calculated by OEDGE global simulation (solid) and by DEGAS 2 interpretation of ENDD data (dotted) [13]. (For interpretation of the references to colour in this figure legend, the reader is referred to the web version of this article.)

for target electron temperatures from 1.25 to 50 eV (i.e. 1/4 to 10 times the baseline T_e, and thus electron pressure), at the measured target density and assuming $T_{i,target} = T_{e,target}$.

Fig. 3a shows the outer wall-integrated carbon mass loss versus $T_{e,target}$, and it is notable that the integrated erosion rate decreases with $T_{e,target}$ below about 30 eV before rising slightly at higher temperatures. This is contrary to intuition given the increase in global particle flux with temperature (ion flux $\sim nT^{1/2}$) [17]. Fig. 3b examines erosion profiles along the outer wall for $T_{e,target} = 2.5$, 5, 20, and 50 eV, and confirms that the sputtering rate decreases with $T_{e,target}$ at almost every location on the outer wall. At the outer target ($s = 1.87$–1.94 m), sputtering rates increase with $T_{e,target}$ (off vertical scale of Fig. 3b), as expected from ion flux scaling.

This counterintuitive outer wall scaling is due to an increase in neutral opacity in the divertor. At divertor-relevant T_e the deuterium ionization rate is a strong function of T_e, so neutrals in the hot divertor are ionized and swept to the target before they

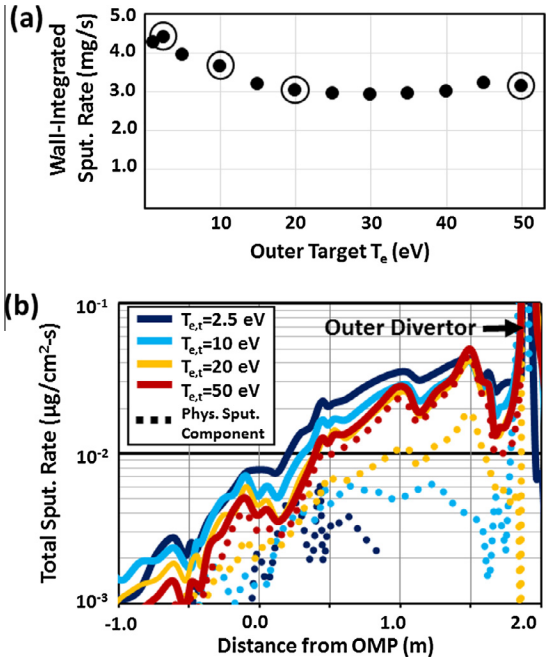

Fig. 3. (a) Sputtering rate integrated across the outer wall ($s = -2.0$ to 1.866), as function of outer target T_e ($\sim P_e$). (b) Poloidal profiles of sputtered flux for cases circled in (a). Solid lines denote physical + chemical sputtering, while dotted denote only physical component.

can escape the divertor region. Fig. 4 shows the ionization mean-free-path (λ_{iz}) for a deuterium atom at the local ion temperature for the $T_{e,target}$ = 5 eV case and the $T_{e,target}$ = 20 eV case; the hotter case features a wide swath of sub-cm λ_{iz}, forming a barrier that neutrals are unlikely to cross without ionizing. This reduces the neutral flux to the wall, and thus the chemical erosion rate. These trapped neutrals still strike the outer target as ions, and across this $T_{e,target}$ scan there is a strong secular increase in outer target-integrated mass loss, from 0.2 mg/s at 1.25 eV, to 6.9 mg/s at 10 eV, up to 134 mg/s at 50 eV.

The slight increase in outer wall erosion at high $T_{e,target}$ arises due to the onset of physical sputtering by neutrals above the threshold sputtering energy of 28 eV. Although the neutral flux to the wall drops continuously with temperature/pressure, the energy of these neutrals increases; we can see from the physical sputtering components of the profiles in Fig. 3b that physical sputtering goes from negligible in low $T_{e,target}$ cases to dominant at high $T_{e,target}$.

This analysis was also carried out by scaling the target density (at constant temperature), and similar results were obtained. This is because OSM tends to calculate a similar temperature profile in order to conserve energy along the ring, so a similar high-ionization region forms to keep the neutrals in the divertor.

4. Dependence on wall and target recycling

Thin lithium coatings have been used as a wall conditioning technique in NSTX, and interpretive modeling with SOLPS has shown that data from Li-coated discharges are consistent with an outer target recycling coefficient that has been reduced from R = 0.98 to R = 0.9 [18]. This sensitivity scan investigates the effect that such a reduction in recycled neutrals would have on erosion at the outer wall.

The ballistically reflected component (R_{refl}) of the recycling coefficient is a sensitive function of incident energy and angle, so it is calculated using TRIM results for deuterium on carbon. Introducing mixed-material lithium effects would yield a more accurate local sputtering yield, but is beyond the scope of this study. Total recycling coefficients between R = 0.8 and R = 1.0 are obtained by modifying the fraction of neutrals that are thermally desorbed (R_{therm}) so that $R_{refl} + R_{therm} = R$.

Reducing recycling lowers the neutral pressure along all parts of the outer wall, reducing the population available for CX collisions and thus consistently reducing the carbon sputtered from each location. The outer wall-integrated mass loss rate is found to monotonically decrease with R, as shown in Fig. 5. Simulations are run with reduced recycling applied to all PFC elements (blue diamonds), or applied only to the outer target (red squares), intended to represent uniform lithium evaporation and a dedicated lithium divertor module, respectively. We see that ~75% of the reduction in mass loss rate is reproduced by only reducing recycling at the outer target, indicating that the majority of wall-directed neutrals originated at the divertor.

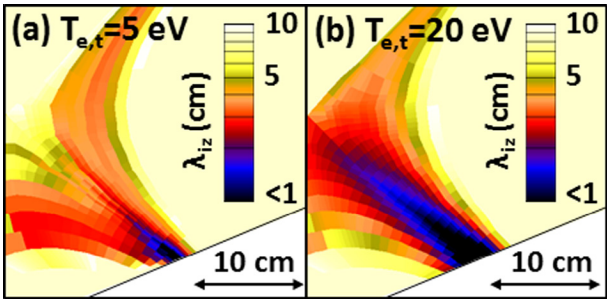

Fig. 4. Calculated ionization mean free path (λ_{iz}) for D^0 (assuming $T_{D0} = T_i$) at outer divertor leg for (a) target T_e = 5 eV, and (b) target T_e = 20 eV.

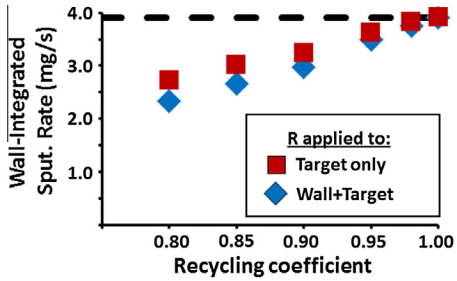

Fig. 5. Sputtering rate integrated across the outer wall (s = −2.0 to 1.866), as function of recycling coefficient R. Blue diamonds: modified R applied to all surfaces; Red squares: modified R applied only to outer target, R = 1.0 elsewhere. (For interpretation of the references to colour in this figure legend, the reader is referred to the web version of this article.)

5. Dependence on low-field-side gas puffing

Low-field side gas puffs, used for fueling and diagnostic purposes, have a direct effect on outer wall erosion since a large neutral population is introduced directly in front of the material surface, without any divertor opacity effects to reduce the flux to the wall. Here, erosion due to a molecular deuterium gas puff at the outer midplane is estimated, in an approximation of the puff used in the NSTX Gas Puff Imaging (GPI) diagnostic [19].

Due to the 2D axisymmetric nature of the OSM solver used in this study, the gas puff source is modeled as a toroidally continuous tube rather than a more realistic finite source. Despite this limitation, upper and lower bounds for the erosion profile can be calculated by scaling the gas rate of the toroidal puff. The modeled toroidal gas puff is set to match the measured GPI peak puff rate of 3.3×10^{21} D_2/s, in order to match the number of particles introduced to the machine and thus provide a lower bound on the erosion rate near the puff duct. The GPI puff duct has a toroidal extent of ~20 cm (out of a toroidal midplane circumference of 9.8 m), so scaling the toroidal puff rate up to 1.6×10^{23} D_2/s matches the particle flux introduced in front of the surface and will provide an upper bound on the erosion rate. The simulated poloidal erosion profiles for both cases, as well as the no-puff case, are shown in Fig. 6.

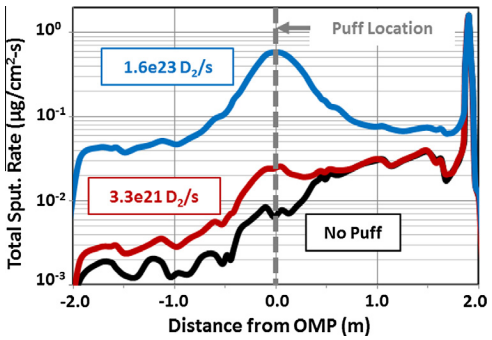

Fig. 6. Poloidal profiles of sputtered flux due to toroidally-continuous gas puff from outer midplane. A puff rate of 3.3e21 D_2/s (red) matches number of particles introduced by toroidally-finite GPI puff, while puff rate of 1.6e23 D_2/s (blue) matches particle flux in front of GPI puff duct. (For interpretation of the references to colour in this figure legend, the reader is referred to the web version of this article.)

Even in the lower bound case, a noticeable increase in neutral pressure and thus chemical sputtering-dominated erosion rate is found in the vicinity of the puff. Limiting this new erosion rate to the toroidal extent of the puff duct, the integrated mass loss rate increases from 3.9 mg/s to 4.0 mg/s. The local change in erosion is much more drastic in the upper bound case, and the wall-integrated rate increases to 4.9 mg/s.

The lower bound case effectively models the extreme of all puffed particles instantaneously spreading toroidally, while the upper bound case models all puffed particles staying directly in front of the puff duct. Due to finite toroidal spreading the actual erosion profile will lie somewhere between these extremes. In addition, this simulation only models the peak rate, while the flow rate of gas puffs typically falls off exponentially as the plenum empties. A more complete analysis of erosion from gas puffs will require a three-dimensional, time-dependent treatment.

6. Conclusions

OEDGE modeling shows that modification of the neutral pressure in front of the wall surface is the driving factor behind changes in erosion rate from the carbon wall of NSTX, due to the dominance of chemical sputtering. Despite a global increase in particle flux, the neutral flux to and thus erosion rate from the outer wall is found to decrease with divertor plasma pressure (a proxy for input power) at low to medium divertor temperatures, owing to the growth of regions of high ionization that impede the flight of recycled neutrals to the outer wall. At high plasma pressures the erosion rate climbs (even as the neutral flux drops), as physical sputtering becomes the dominant erosion mechanism.

Direct modification of recycling coefficients show that neutrals recycled from the divertor are the primary source of particles striking the outer wall, while neutrals recycled from the wall itself are a secondary source. For example, a 10% reduction in recycling from the outer target drops the outer wall erosion rate from 3.9 mg/s to 3.2 mg/s, but this only extrapolates to 3.0 mg/s when the same reduced recycling is applied to the entire machine. Even small amounts of erosion from the outer wall can be an important source of core impurities, so this further motivates the investigation of low-recycling regimes.

OEDGE simulations show that gas puffing on the low-field-side greatly increases the neutral pressure in front of the puff duct and leads to enhanced erosion near the puff. Rudimentary simulations suggest that a midplane D_2 puff, continuously running at the peak rate of the GPI puff (3.3×10^{21} D_2/s), will increase the outer wall erosion rate by 0.1–1.0 mg/s. However, time-dependent 3D simulations are necessary to more precisely analyze the erosive effects of gas injection from finite sources.

Future work will extend the plasma grid towards the wall through the far SOL. This will capture outer wall erosion due to ion impact, as well as far SOL particle drifts and flows. Experiments are also planned on NSTX-U to compare to erosion simulations.

Acknowledgements

This work has been supported by US Dept. of Energy contract DE-AC02-09CH11466. JHN and TA have been supported in part by the US DOE Fusion Energy Sciences Fellowship.

References

[1] P.C. Stangeby, J. Nucl. Mater. 415 (2011) S278–S283.
[2] P.C. Stangeby, Nucl. Fusion 51 (2011) 063001.
[3] J.P. Coad, Nucl. Fusion 46 (2006) 350–366.
[4] J.P. Coad, Phys. Scripta T145 (2011) 014003.
[5] J.D. Elder, J. Nucl. Mater. 390–391 (2009) 376–379.
[6] V. Rohde, Phys. Scripta T111 (2004) 49–54.
[7] M.A. Jaworski, Nucl. Fusion 53 (2013) 083032.
[8] J.E. Menard, Nucl. Fusion 52 (2012) 083015.
[9] T. Tanabe, J. Nucl. Mater. 438 (2013) S19–S26.
[10] D. Reiter, Fusion Sci. Technol. 47 (2005) 172–186.
[11] P.C. Stangeby, J. Nucl. Mater. 313–316 (2003) 883–887.
[12] J. Kallman, Rev. Sci. Instrum. 81 (2010) 10E117.
[13] M.A. Jawoski, J. Nucl. Mater. 438 (2013) S384–S387.
[14] D.P. Stotler (these proceedings).
[15] W. Eckstein, Sputtering yields, in: Sputtering by Particle Bombardment, Springer, 2007, pp. 33–187.
[16] W. Jacob, J. Roth, Chemical sputtering, in: Sputtering by Particle Bombardment, Springer, 2007, pp. 329–400.
[17] P.C. Stangeby, The Plasma Boundary of Magnetic Fusion Devices, Taylor & Francis, 2000.
[18] J.M. Canik, J. Nucl. Mater. 415 (2011) S409–S412.
[19] S.J. Zweben, Nucl. Fusion 44 (2004) 134–153.